Geosci. Model Dev. Discuss., 7, 741–775, 2014
www.geosci-model-dev-discuss.net/7/741/2014/
doi:10.5194/gmdd-7-741-2014

Geoscientific Model Development Discussions
Open Access

Simultaneous parameterization of the two-source evapotranspiration model by Bayesian approach: application to spring maize in an arid region of northwest China

G. F. Zhu[1], X. Li[2], Y. H. Su[2], K. Zhang[1], Y. Bai[1], J. Z. Ma[1], C. B. Li[1], X. L. Hu[2], and J. H. He[1]

[1]Key Laboratory of Western China's Environmental Systems (Ministry of Education), Lanzhou University, Lanzhou 730000, China
[2]Cold and Arid Regions Environmental and Engineering Research Institute, Chinese Academy of Science, Lanzhou 730000, China

Received: 12 December 2013 – Accepted: 10 January 2014 – Published: 21 January 2014

Correspondence to: G. F. Zhu (zhugf@lzu.edu.cn)

Published by Copernicus Publications on behalf of the European Geosciences Union.

Abstract

Based on direct measurements of half-hourly canopy evapotranspiration (ET; $W m^{-2}$) using the eddy covariance (EC) system and daily soil evaporation (E; $mm d^{-1}$) using microlysimeters over a crop ecosystem in arid northwest China from 27 May to 14 September in 2013, a Bayesian method was used to simultaneously parameterize the soil surface and canopy resistances in the Shuttleworth–Wallace (S–W) model. The posterior distributions of the parameters in most cases were well updated by the multiple measuring dataset with relatively narrow high-probability intervals. There was a good agreement between measured and simulated values of half-hourly ET and daily E with a linear regression being $y = 0.84x + 0.18$ ($R^2 = 0.83$) and $y = 1.01x + 0.01$ ($R^2 = 0.82$), respectively. The causes of underestimations of ET by the S–W model was mainly attributed to the micro-scale advection, which can contribute an added energy in the form of downward sensible heat fluxes to the ET process. Therefore, the advection process should be taken into accounted in simulating ET in heterogeneous land surface. Also, underestimations were observed on or shortly after rainy days due to direct evaporation of liquid water intercepted in the canopy. Thus, the canopy interception model should be coupled to the S–W model in the long-term ET simulation.

1 Introduction

In agriculture ecosystem, more than 90 % of all water inputs is lost by evapotranspiration (ET) (Morison et al., 2008), which is defined as the sum of water loss by evaporation (E) from soil and transpiration (T) from plants (Rana and Katerji, 2000). E and T are influenced by different abiotic and biotic factors (Wang and Yakir, 2000), and the contributions of E and T to the total ecosystem ET are highly variable in space and time (Ferretti et al., 2003). Thus, accurate measurement or estimation of ET and its components (E and T) is essential for many applications in agriculture, such as irrigation scheduling, drainage, and yield forecasts (Wallace and Verhoef, 2000; Flumignan et al.,

GMDD
7, 741–775, 2014

2011; Sun et al., 2012). The Shuttleworth–Wallace model (S–W model) (Shuttleworth and Wallace, 1985) takes the interactions between the fluxes from soil and canopy into account, and is physically sound and rigorous. Previous studies have proved that it has good performances for row crops such as maize, wheat, cotton, sorghun and vine (Stannard, 1993; Tourula and Heikinheimo, 1998; Anadranistakis et al., 2000; Teh et al., 2001; Lund and Soegaard, 2003; Kato et al., 2004; Ortega-Farias et al., 2007; Zhang et al., 2008).

Despite these studies, there are still some insufficiencies in the application of the S–W model (Hu et al., 2009; Zhu et al., 2013). First, the S–W model is sensitive to the errors in the values of canopy and soil resistances (Lund and Soegaard, 2003). Previous studies mainly focused on the parameterization of the canopy resistance (Hanan and Prince, 1997; Samanta et al., 2007; Zhu et al., 2013), and less attentions has been committed to the parameterization of the soil surface resistance (Sellers et al., 1992; van de Griend and Owe, 1994; Villagarcía et al., 2010). In crop ecosystem, E may contribute significantly to the total ET when leaf area index (LAI) is low (Lund and Soegaard, 2003; Zhang et al., 2008). Thus, simultaneous parameterization of the canopy and soil resistances in the S–W model, based on direct measurement of ET and its components by using a combination of micro-meteorological (e.g. eddy covariance methods, Bowen ratio), hydrological (e.g. chambers, microlysimeters) and eco-physiological techniques (e.g. sap-flow, stable isotopes) (Williams et al., 2004; Scott et al., 2006), is important to reduce the model error. However, such studies are relative rare or non-existent. Secondly, as far as the parameterization method is concerned, abundant evidence has shown that the Bayesian method provides a powerful new tool to simultaneously optimized many or all model parameters against all available measurements (Clark and Gelfand, 2006). Although some pioneering efforts have been made (e.g. Samanta et al., 2007; Zhu et al., 2013), the Bayesian method has been much less frequently used in parameterization of ET model than in the other environmental sciences (van Oijen et al., 2005). Moreover, the Bayesian method, to our knowledge, has not been used to simultaneously optimized the parameters of the S–W

GMDD
7, 741–775, 2014

model against multiple measuring dataset (Sect. 2.5). Finally, arid northwest China, one of the driest area in the world (Zhu et al., 2007, 2008), is characterized by a widely distributed desert/Gobi interspersed with many oases in different sizes and shapes. Land surface processes of this heterogeneous region are much complex than in other regions (Zhang and Huang, 2004). Thus, the applicability of the S–W model in such regions need to be investigated in details.

Based on direct measurements of different components of ET obtained by using the eddy covariance technique and microlysimeters over a spring maize field in arid region of northwest China from 27 May to 14 September in 2013, the objectives of the present study were to: (1) simultaneously parameterize the S–W model using the Bayesian method against multiple measuring dataset; (2) verify the performances of the S–W model, and identify the causes of failure and success in simulating ET over the crop ecosystem in arid desert oasis of northwest China. It is expected that this study can not only promote the developments of ET model parameterization, but also help us to find a proper direction in modifying the S–W model used in arid regions.

2 Materials and methods

2.1 Study site

The study site is located in Daman (DM) Oasis, in the middle Heihe River Basin, Gansu province, China (100°22′20″ E, 38°51′20″ N; 1556 m a.s.l.; Fig. 1). The annual average temperature and precipitation was 7.2 °C and 125 mm (1960–2000), respectively. The potential evaporation is around 2365 mm yr^{-1}, and the dryness index is 15.9. The soil type is silt clay loam on the surface and silt loam in the deeper layer.

The study area has an agricultural development history of over 2000 yr owing to its flat terrain, adequate sunlight and convenient water resources from Qilian Mountains. The main crops in the DM Oasis are spring wheat and maize. The spring wheat (*Triticum aestivum* L.) is generally sown in the later March and harvested in the middle

GMDD
7, 741–775, 2014

10 days of July, while the maize (*Zea mays* L.) is sown in the late April and harvested in the middle 10 days of September.

2.2 Measurements and data processing

The field observation systems at this site were constructed in May 2013 as part of the Heihe Watershed Allied Telemetry Experimental Research (HiWATER) project (see details in Li et al., 2013b). The fluxes of sensible heat (H), latent heat (λET) and carbon dioxide were measured at the height 4.5 m using the eddy covariance (EC) system (Liu et al., 2014), which consists of an open-path infrared gas analyzer (Li-7500, LiCor Inc., Lincoln, NE, USA) and a 3-D sonic anemometer (CSAT-3, Campbell Scientific Inc., Logan, UT, USA). The EC data were sampled at a frequency of 10 Hz by a data logger (CR5000, Campbell Scientific Inc.), and then were processed with an average time of 30 min. Post-processing calculations, using EdiRe software, included spike detection, lag correction of H_2O/CO_2 relative to the vertical wind component, sonic virtual temperature conversion, planar fit coordinate rotation, the WPL density fluctuation correction and frequency response correction (Xu et al., 2014). Data gaps due to instrument malfunction, power failure and bad weather conditions were filled using artificial neural network (ANN) and mean diurnal variations (MDV) methods (Falge et al., 2001). The ANN method was applied when the synchronously meteorological data were available; otherwise, the MDV method was used. The gap-filling data were used only to analyze the seasonal and annual variations in ET.

Continuous complementary measurements also included standard hydrometeorological variables. Rainfall was measuring using a tipping bucket rain gauge (TE525MM, Campbell Scientific Instruments Inc.). Air temperature and relative humidity (HMP45C, Vaisala Inc., Helsinki, Finland) and wind speed/direction (034B, Met One Instruments, Inc. USA) were measured at heights of 3, 5, 10 15, 20, 30 and 40 m above the ground. Downward and upward solar and longwave radiation (PSP, The EPPLEY Laboratory Inc., USA) and photosynthetic photon flux density (PPFD) (LI-190SA, LI-COR Inc.) were measured at height of 6 m. Soil temperature

GMDD
7, 741–775, 2014

(Campbell-107, Campbell Scientific Instruments Inc.) and moisture (CS616, Campbell Scientific Instruments Inc.) were measured at 0.02, 0.04, 0.1, 0.2, 0.4, 0.8, 1.2 and 1.6 m depths. Three heat flux plates (HFT3, Campbell Scientific Instruments Inc.) were randomly buried at the depths of 0.01 m. The average soil heat fluxes were calculated using the three randomly buried plates. These data were logged every 10 min by a digital micrologger (CR23X, Campbell Scientific Inc.) equipped with an analog multiplexer (AM416) was used for sampling and logging data.

Daily soil evaporation was measured using three microlysimeters randomly placed between crop rows. The microlysimeters with an internal diameter of 10 cm and a depth of 20 cm were filled with an intact soil core and pushed into soil with the top slightly above the soil surface (Daamen et al., 1993; Liu et al., 2002). The average weight loss of these microlysimeters measured using electronic scales with 0.01 g precision was nearly equal to soil evaporation. In order to keep the soil moisture in microlysimeters similar to that between the rows, the soil in the microlysimeters was replaced daily or every two days.

Leaf area index (LAI) was measured using AM300 portable leaf area meter (ADC BioScientific Ltd., UK). The fraction of land cover (f) was estimated by measuring the projected crop canopy area of selected stands in corresponding field plot. LAI, f and crop height were measured approximately every 10 days during the growing season, and the gaps were linearly interpolated to daily interval.

2.3 Description of the S–W model

In the S–W model, the ecosystem evapotranspiration (λET; W m^{-2}) is separated into evaporation from the soil surface (λE; W m^{-2}) and transpiration from the vegetation canopy (λT; W m^{-2}) (Fig. 2), which are calculated as (Shuttleworth and Wallace, 1985; Lhomme et al., 2012):

$$\lambda \mathrm{ET} = \lambda E + \lambda T = C_\mathrm{s}\mathrm{ET}_\mathrm{s} + C_\mathrm{c}\mathrm{ET}_\mathrm{c} \quad (1)$$

GMDD
7, 741–775, 2014

$$ET_s = \frac{\Delta A + [\rho C_p D - \Delta r_a^s (A - A_s)]/(r_a^a + r_a^s)}{\Delta + \gamma[1 + r_s^s/(r_a^a + r_a^s)]} \quad (2)$$

$$ET_c = \frac{\Delta A + [\rho C_p D - \Delta r_a^c A_s]/(r_a^a + r_a^c)}{\Delta + \gamma[1 + r_s^c/(r_a^a + r_a^c)]} \quad (3)$$

$$C_s = \frac{1}{1 + [R_s R_a/R_c(R_s + R_a)]} \quad (4)$$

$$C_c = \frac{1}{1 + [R_c R_a/R_s(R_c + R_a)]} \quad (5)$$

$$R_a = (\Delta + \gamma) r_a^a \quad (6)$$

$$R_c = (\Delta + \gamma) r_a^c + \gamma r_s^c \quad (7)$$

$$R_s = (\Delta + \gamma) r_a^s + \gamma r_s^s \quad (8)$$

$$\lambda E = \frac{\Delta A_s + \rho C_p D_0 / r_a^s}{\Delta + \gamma(1 + r_s^s/r_a^s)} \quad (9)$$

$$\lambda T = \frac{\Delta(A - A_s) + \rho C_p D_0 / r_a^c}{\Delta + \gamma(1 + r_s^c/r_a^c)} \quad (10)$$

$$D_0 = D + \frac{(\Delta A - (\Delta + \gamma)\lambda \mathrm{ET}) r_a^a}{\rho c_p} \quad (11)$$

where ET_s, and ET_c are terms to describe evaporation from soil and transpiration from the plant ($W m^{-2}$), respectively; C_s and C_c are soil surface resistance coefficient and canopy resistance coefficient (dimensionless), respectively; λ is the latent heat of evaporation ($J kg^{-1}$); Δ is the slope of the saturation vapor pressure vs. temperature curve ($kPa K^{-1}$); ρ is the air density ($kg m^{-3}$); C_p is the specific heat capacity of dry air ($1013 J kg^{-1} K^{-1}$); D and D_0 (kPa) is the air water vapor pressure deficit at the reference height (3 m) and the canopy height, respectively; γ is the psychrometric constant

GMDD
7, 741–775, 2014

(kPa K^{-1}); r_s^c and r_s^s are the surface resistance for plant canopy and soil surface (s m^{-1}), respectively; $r_a^c$and r_a^s are aerodynamic resistances from the leaf to canopy height and soil surface to canopy height (s m^{-1}), and r_a^a is aerodynamic resistances from canopy height to reference height (s m^{-1}). A and A_s (W m^{-2}) are the available energy input above the canopy and above the soil surface, respectively, and are calculated as:

$$A = R_n - G \quad (12)$$

$$A_s = R_{ns} - G \quad (13)$$

where R_n and R_{ns} are net radiation fluxes into the canopy and the substrate (W m^{-2}), respectively; G is the soil heat flux (W m^{-2}). R_{ns} was calculated using a Beer's law relationship of the form:

$$R_{ns} = R_n \exp(-K_A \mathrm{LAI}) \quad (14)$$

in which K_A is the extinction coefficient of light attenuation, and is approximately 0.41 for spring maize (Mo et al., 2000).

The climate-related variables (i.e., λ, e_s, Δ, ρ and γ) in Eqs. (1)–(3) is calculated by the formulas of Allen et al. (1998).

2.4 Calculation of resistances in the S–W model

The resistance network of the S–W model is shown in Fig. 2. In this paper, the three aerodynamic resistance (i.e., r_a^a, r_a^c and r_a^s) were calculated using the same approach suggested by Shuttleworth and Wallace (1985), Shuttleworth and Gurney (1990) and Lhomme et al. (2012).

The canopy resistance (r_s^c), which is the equivalent resistance of all the individual stomates in a canopy and depends on the environmental variables, can be calculated using the Jarvis-type model (Jarvis, 1976)

GMDD
7, 741–775, 2014

$$r_s^c = \frac{r_{STmin}}{2LAI\prod_i F_i(X_i)} \tag{15}$$

where r_{STmin} represents the minimal stomatal resistance of individual leaves under optimal conditions. $F_i(X_i)$ is the stress function of a specific environmental variable X_i, with $0 \le F_i(X_i) \le 1$. Following Stewart (1998) and Verhoef and Allen (2000), the stress functions were expressed as:

$$F_1(R_s) = \frac{R_s}{1000}\frac{1000 + k_1}{R_s + k_1} \tag{16}$$

$$F_2(T_a) = \frac{(T_a - T_{a,min})(T_{a,max} - T_a)^{(T_{a,max}-k_2)/(k_2-T_{a,min})}}{(k_2 - T_{a,min})(T_{a,max} - k_2)^{(T_{a,max}-k_2)/(k_2-T_{a,min})}} \tag{17}$$

$$F_3(D) = 1 - k_3 D \tag{18}$$

$$F_4(\theta_r) = \begin{cases} 1 & \theta_r > \theta_{cr} \\ \frac{(\theta_r - \theta_{wp})}{(\theta_{cr} - \theta_{wp})} & \theta_{wp} \le \theta_r \le \theta_{cr} \\ 0 & \theta_r < \theta_{wp} \end{cases} \tag{19}$$

where $k_1 - k_3$ are constants (units see Table 1); R_s is the incoming solar radiation ($W\,m^{-2}$); T_a is the air temperature (°C) at the reference height; $T_{a,min}$ and $T_{a,max}$ are the lower and upper temperatures limits (°C), respectively, which are T_a values when $F_2(T_a) = 0$ and are set at values of 0 and 40 °C (Harris et al., 2004); θ_r is the actual volumetric soil water content in the root-zone at depth of 0–60 cm ($m^3\,m^{-3}$); θ_{wp} is water content at the wilting point ($m^3\,m^{-3}$); and θ_{cr} is the critical water content at which plant stress starts and was set as $0.30\,m^3\,m^{-3}$ in this study.

GMDD
7, 741–775, 2014

The soil surface resistances (r_s^s; Fig. 2) was expressed as a function of near-surface soil water content (Sellers, 1992; Verhoef et al., 2006, 2012; Zhu et al., 2013):

$$r_s^s = \exp(b_1 - b_2 \frac{\theta_s}{\theta_{sat}}) \quad (20)$$

in which b_1 and b_2 are empirical constants (s m^{-1}); θ_s is soil water content in the top layer of soil (at depth of 2 cm); θ_{sat} is the saturated soil water content (m^3 m^{-3}), which was estimated empirically through the near-surface soil texture. In summary, there are 6 site- and species-specific parameters needed to be estimated in the S–W model associated with soil and canopy resistances, which are b_1, b_2, r_{STmin} and $k_1 - k_3$.

2.5 Model calibration and evaluation

A Bayesian approach was applied to simultaneously estimate the parameters associated with the soil (b_1, b_2) and canopy ($r_{ST\,min}, k_1, k_2, k_3$) resistances in the S–W model (van Oijen et al., 2005; Svensson et al., 2008; Zhu et al., 2011, 2013). The two dataset used to simultaneously optimize the parameter values were: EC-measured half-hourly evapotranspiration (λET; W m^{-2}) and microlysimeters-measured daily soil evaporation (E; mm d^{-1}).

Corresponding to each of the data sets (e.g., λET and E), the model error $e_i(t)$ ($i = 1,2$) is expressed by:

$$e_i(t) = O_i(t) - f_i(t) \quad (21)$$

where $O_i(t)$ and $f_i(t)$ is observed and modeled (Eqs. 1 and 9) values of the ith dataset at time t, respectively. Assuming the model error $e_i(t)$ follows a Gaussian distribution with a zero mean, the data likelihood function can be expressed by:

$$p(O|c) \propto \exp\left\{ -\sum_{i=1}^{m} \frac{1}{2\sigma_i^2} \sum_{t=1}^{n_i} (e_i(t))^2 \right\} \quad (22)$$

GMDD
7, 741–775, 2014

where c is the parameter vector; O is the observed data sets; m is the number of dataset (= 2 in this study); σ_i^2 (i = 1,2) is the measurement error variance of the ith dataset; n_i is the number of observations of ith dataset. Then with Bayes' theorem, the posterior distribution of parameters c is generated by:

$$p(c|O) \propto p(O|c)p(c) \tag{23}$$

where $p(c)$ represents prior probability distributions of parameters c, and $p(c|O)$ is the posterior distributions of parameters c. The posterior distribution was sampled using the Metropolis–Hasting (M–H) algorithm (Metropolis et al., 1953; Hastings, 1970), a version of the Markov Chain Monte Carlo (MCMC) technique. To generate a Markov chain in the parameter space, the M–H algorithm was run by repeating two steps: a proposing step and a moving step. In the proposing step, a candidate point c^{new} is generated according to a proposal density $P(c^{\text{new}}|c^{k-1})$, where c^{k-1} is the accepted point at the previous step. In the moving step, point c^{new} is treated against the Metropolis criterion to examine if it should be accepted or rejected (see Zhu et al., 2011, 2013 for detailed description on MCMC sampling procedure). We ran at least three parallel MCMC chains with 20 000 iterations each, evaluated the chains for convergence (Gelman and Rubin, 1992), and thinned the chains (every 20th iteration) when appropriate to reduce within chain autocorrelation, thereby producing an independent sample of 3000 values for each parameter from the joint posterior distribution.

During the whole growing season, the measurements were split into two independent dataset by taking alternate days. The model parameters were derived using one dataset. Then the optimized S–W model was used with the second data set to predict the different components of ET and these values were compared to the measured values in the second dataset. The performance of the S–W model was evaluated using the coefficient of determination of the linear regression between measured and estimated values of water vapor fluxes, R^2, representing how much the variation in the observations was explained by the models. Also, the root mean square error (RMSE),

GMDD
7, 741–775, 2014

mean bias error (MBE), index of agreement (IA) and model efficiency (EF) (Legates and McCabe, 1999; Poblete-Echeverria and Ortega-Farias, 2009) were included in the statistical analysis, which are calculated as follows:

$$\mathrm{RMSE} = \sqrt{\frac{1}{n}\sum_{t=1}^{n}[O(t) - f(t)]^2} \tag{24}$$

$$\mathrm{MBE} = \frac{1}{n}\sum_{t=1}^{n}[O(t) - f(t)] \tag{25}$$

$$\mathrm{IA} = 1 - \frac{\frac{1}{n}\sum_{t=1}^{n}[O(t) - f(t)]^2}{\sum_{t=1}^{n}[|O(t) - \overline{O}| + |f(t) - \overline{O}|]^2} \tag{26}$$

$$\mathrm{EF} = 1 - \frac{\sum_{t=1}^{n}[O(t) - f(t)]^2}{\sum_{t=1}^{n}[O(t) - \overline{O}]^2} \tag{27}$$

where n is the total number of observations, $O(t)$ is the observed values at time t, $\overline{O}$ is the mean of the observed values, and $f(t)$ is the simulation which was calculated using the posterior expectancy of parameter.

3 Results and discussion

3.1 Environmental and biological factors

Detailed information on the seasonality of key environmental and biological variables is essential to assess seasonal variation in the actual ET and its partitioning. The

GMDD
7, 741–775, 2014

seasonal change in net solar radiation (R_n; MJ m^{-2} d^{-1}), air temperature (T_a; °C), air water vapor pressure deficit (D; kPa), wind speed (u, m s^{-1}) at the height of 3 m, rainfall and irrigation (mm), soil water content (θ; m^3 m^{-3}), and leaf area index (LAI; m^2 m^{-2}) was illustrated in Fig. 3. During the study period (DOY147-257), the daily mean R_n varied from 2.6 to 18.5 MJ m^{-2} d^{-1} with an average value of 11.9 MJ m^{-2} d^{-1}. The peaked values were recorded from the end of June to the middle of July (DOY180-195). The variation of mean daily air temperature (T_a) has a similar trend to R_n, varying from 8.8 to 24.9 °C with an average value of around 19.0 °C. D exhibited large diurnal variation ranging from 0 to 3.5 kPa, and the daily mean D was relative small when the LAI was larger than 3 m^2 m^{-2} (DOY197-230). Daily mean wind speed (u) ranged from 0.5 to 3.2 m s^{-1}, and was close to normal long-term values. Total precipitation during the study period was 104.2 mm with eight events over 5.0 mm (Fig. 3). θ varied greatly over the whole growing season. The variability of θ mainly depended on irrigation scheduling of local government (irrigation quota and timing). Soil water content had a peak value (about 0.35 m^3 m^{-3}) after irrigation and gradually reduced till the next irrigation (Fig. 3). The LAI showed a clear "one peak" pattern over the whole growing season with relative high values of 3.5 m^{-2} m^{-2} from early July to late August (DOY184-221).

3.2 Posterior distribution of S–W model parameters

The posterior parameter distributions are shown as histograms in Fig. 4 and summarized in Table 1 by posterior means and 95 % probability intervals. The results showed that the Bayesian calibration against the multiple dataset was in most cases successful in reducing the assumed prior ranges of the parameters values. Among the parameters, r_{STmin} has the least posterior variability relative to its prior range, followed by b_1, b_2, k_2 (approximately symmetric with distinctive modes; Fig. 4), while parameters k_1 and k_3 have relative large variability (widely spread on the prior bounds). Ortega-Farias et al. (2007) have demonstrated that the S–W model is very sensitive to errors in r_{STmin}, and much less to uncertainties in other parameters. Thus, we thought that

GMDD
7, 741–775, 2014

the key parameters in the S–W model were well estimated by the Bayesian method against the multiple measuring dataset. In addition, the six calibrated parameters were not significantly inter-correlated with each other except for the pair b_1 and b_2, which was positively correlated with a correlation coefficient of 0.85.

The responses of soil surface resistances (r_s^s) to soil water content computed using our posterior mean b_1 and b_2 values were very similar to that calculated using equation developed by Ortega-Farias et al. (2010) based on direct soil evaporation measurements, but seemed to be more sensitive to changes in soil water contents compared with some other studies (e.g., Sun, 1982; Sellers, 1992; Zhu et al., 2013; Fig. 5). The posterior mean value of r_{STmin} from our study was very close to that (20 s m^{-1}) reported for spring maize growing in northwest China obtained by using the least squares fitting method (Li et al., 2013a). The variations of the minimal stomatal resistance (r_{STmin}) for many natural and cultivated plantshave been widely investigated by previous studies (Korner et al., 1979; Pospisilova and Solarova, 1980). Typical values for r_{STmin} vary considerably from about 20–100 s m^{-1} for crops to 200–300 s m^{-1} for many types of trees. Thus, our results fell within the range of previous studies.

3.3 Model performance compared with measurements

Having parameterized the S–W model as described above, we ran the model to simulate the half-hourly λET (Eq. 1) and λE (Eq. 9) values (W m^{-2}). The daily estimations of evapotranspiration (ET; mm d^{-1}) and soil evaporation (E; mm d^{-1}) was obtained by summing up the half-hourly simulated values. The statistical analysis of observed vs. estimated values of water vapor fluxes at different time-scales were summarized in Table 2. These results indicated that the parameterized S–W model was able to predicate λET on a half-hourly basis with values of R^2, IA and EF equal to 0.83, 0.93 and 0.74, respectively. However, there still existed the difference between measured and modeled half-hourly λET values for the spring maize in the arid desert oasis. The slope (0.84) of regressive equation between the measured and modeled half-hourly λET values was lower than one (Table 2 and Fig. 6a), which indicated that the S–W

GMDD
7, 741–775, 2014

model tended to underestimate the half-hourly λET with a MBE value of 24.2 W m^{-2}. Ortega-Farias et al. (2010) also reported that the S–W model underestimated on half-hourly time intervals compared the EC-measured λET over a drip-irrigated vineyard in Mediterranean semiarid region during the growing season in 2006. On the contrary, some studies showed that the S–W model overestimated half-hourly λET (e.g., Li et al., 2013a; Ortega-Farias et al., 2007; Zhang et al., 2008). Therefore, the performances of the S–W model seemed to be variable for different crops and places, and there is a need to identify the causes that induced the disagreements between observed and modeled values (discussed below).

The fluctuation of measured and estimated daily ET and E was illustrated in Fig. 7. In this case, a good agreement between measured and estimated daily E was obtained with values of R^2, IA and EF equal to 0.82, 0.94 and 0.76 (Table 2). The points in plots of measured-vs.-modeled daily E fell tightly along the 1 : 1 line (slope = 1.01 and intercept = 0.01 with RMSE = 0.05 and MBE = −0.01; Fig. 6b and Table 2). Thus, we thought that the soil resistance in the S–W model was properly parameterized for the spring maize by the measured soil evaporation data. From Fig. 7, we can also observed that the estimated daily ET generally fluctuated tightly with the measured values. The values of RMSE, MBE, IA and EF were equal to 0.05, 0.14 mm d^{-1}, 0.94 and 0.79, respectively (Table 2). However, great underestimations (> 0.5 mm d^{-1}) were observed on 12 days during the study period (111 days). For example, on 5 July, the estimated and measured daily ET was 2.9 and 4.3 mm d^{-1}, respectively (Fig. 7). Thus, the causes of the underestimations of ET by the S–W on these days needed to be carefully checked based on detailed micrometeorological data. This work would help us to modify the model in a correct way and improve the precision of prediction.

GMDD
7, 741–775, 2014

3.4 Identification of the disagreement/agreement between observed and modeled ET values

The diurnal variation of R_n, H and λET (measured and modeled) above the spring maize ecosystem for some selected days was presented in Fig. 8. Resulting from the high surface heterogeneities, one special phenomenon, known as the "oasis effect" (Lemon et al., 1957) or "cold island effect" (Wang et al., 1992; Zhang and Huang, 2004), was often observed on clear days in July and August in the study area and it is characterized as follows: (1) H is very small and even negative (downward) in the afternoon (Fig. 8a–c) due to the micro-scale advection of hot dry air over the desert to crop surface in the oasis. For an example, on 5 July, H was continuously negative from 12 : 00 to 20 : 00 (Fig. 8a). A strong advection process can be distinctly detected from the temperature and relative humidity profiles (Fig. 9a and b), in which the highest temperature occurred at a height of 8–18 m; (2) measured actual λET often exceeded (Fig. 8a) or was equal to (Figs. 8b and c) the local net radiation because of the added energy in the form of downward fluxes of H to the ET process (Evett et al., 2012). Under such conditions, the S–W model significantly underestimated the actual ET values due to the real atmospheric flows do not correspond to its assumption of horizontal homogeneities (Rao et al., 1974). Thus, how to properly representing the advection process in the S–W model should be paid special attentions in simulating ET over crop ecosystems in arid desert oasis in the future studies. In addition to this situation, slight underestimations were also observed on or shortly after rainy days (Fig. 7). For example, the simulated half-hourly λET was lower than that measured by EC after the rainfall event occurred in 13:00 LT on 17 June (Fig. 8d). We thought that the underestimations by the model on or shortly after rainy days were mainly due to ignoring the direct evaporation of liquid water intercepted in the crop canopy, because no downward H and temperature inversion were observed on this day (Figs. 9c and d). Until now, several canopy interception models have been developed (e.g., Rutter et al., 1971; Mulder, 1985; Gash et al., 1995; Bouten et al., 1996). However, many of them

GMDD
7, 741–775, 2014

were developed for simulating the rainfall interception by forest ecosystems, and their suitability for crops need to be further investigated.

On the other hand, the diurnal variation of simulated half-hourly λET by the parameterized S–W model has a similar trend to the measurements on clear and advection-absent days during the whole study periods (Fig. 8e–h). On these days, H was positive (upwards) at day time (Fig. 8e–h) and no temperature inversion was observed (Fig. 9e and f). Thus, we thought that the parameterization schedule adopted in this study worked well. It also demonstrated that the properly parameterized S–W model can be used in simulating and partitioning ET for homogeneous land surface. Hu et al. (2009) reported that the S–W model parameterized by using Monte Carlo method can successfully simulated ET at four uniform grasslands in China; our previous studies (Zhu et al., 2013) also illustrated that parameterized S–W model can be used to simulate and partition ET over a vast alpine grassland in Qinghai-Tibet Plateau.

4 Conclusions

This study illustrated the use of the Bayesian method to simultaneously parameterize a two-source ET model against the multiple measuring dataset for a crop ecosystem in a desert oasis of northwest China. The posterior distributions of the model parameters in most cases can be well constrained by the observations. Generally, the parameterized model has a good performance in simulating and partitioning ET. However, underestimations were observed on days when micro-scale advection occurred. Therefore, in the future studies, special attentions should be given to proper descriptions of the effects of advection on estimating ET for heterogeneous land surface. In addition, the canopy interception model should be coupled with the two-source ET model in long-term simulation.

Acknowledgements. The eddy covariance flux, meteorological, and other data used in this study are from Heihe Watershed Allied Telemetry Experimental Research (HiWATER) (http://heihedata.org/hiwater). We thank all the scientists, engineers and students who participated

GMDD
7, 741–775, 2014

in HiWATER field campaigns. This research was supported by National Natural Science Foundation of China (No. 41 001 242), the Chinese Academy of Sciences Action Plan for West Development Program Project (KZCX2-XB3-15), and New Century Excellent Talents in University of Chinese Ministry of Education (No. NCET-11-0219).

References

Allen, R. G., Pereira, L. S., Raes, D., and Smith, M.: Crop Evapotranspiration – Guidelines for Computing Crop Water Requirements, FAO Irrigation and Drainage Paper, No. 56, FAO, Rome, 1998.

Anadranistakis, M., Liakatas, A., Kerkides, P., Rizos, S., Gavanosis, J., and Poulovassilis, A.: Crop water requirements model tested for crops grown in Greece, Agr. Water Manage., 45, 297–316, 2000.

Bouten, W., Schaap, M. G., Aerts, J., and Vermetten, A. W. M.: Monitoring and modelling canopy water storage amounts in support of atmospheric depositions studies, J. Hydrol., 181, 305–321, 1996.

Clark, J. S. and Gelfand, A. E.: A future for models and data in environmental science, Trends Ecol. Evol., 12, 375–380, 2006.

Daamen, C., Simmonds, L. E., Wallace, J. S., Laryea, K. B., and Sivakumar, M. U. K.: Use microlysimeters to measure evaporation from sandy soils, Agr. Forest Meteorol., 65, 159–173, 1993.

Evett, S. R., Kustas, W. P., Gowda, P. H., Anderson, M. A., Prueger, J. H., and Howell, T. A.: Overview of the Bushland Evapotranspiration and Agricultural Remote sensing EXperiment 2008 (BEAREX08): a field experiment evaluating methods for quantifying ET at multiple scales, Adv. Water Resour., 50, 4–19, 2012.

Falge, E., Baldocchi, D., Olson, R. J., Anthoni, P., Aubinet, M., Bernhofer, C., Burba, G., Ceulemans, R., Clement, R., Dolman, H., Granier, A., Gross, P., Grünwald, T., Hollinger, D., Jensen, N.-O., Katul, G., Keronen, P., Kowalski, A., Ta Lai, C., Law, B. E., Meyers, T., Moncrieff, J., Moors, E., Munger, J. W., Pilegaard, K., Rannik, U ., Rebmann, C., Suyker, A., Tenhunen, J., Tu, K., Verma, S., Vesala, T., Wilson, K., and Wofsy, S.: Gap filling strategies for defensible annual sums of net ecosystem exchange, Agr. Forest Meteorol., 107, 43–69, 2001.

GMDD
7, 741–775, 2014

Ferretti, D., Pendall, E., Morgan, J., Nelson, J., LeCain, D., and Mosier, A.: Partitioning evapotranspiration fluxes from a Colorado grassland using stable isotopes: seasonal variations and ecosystem implications of elevated atmospheric CO_2, Plant Soil, 254, 291–303, 2003.

Flumignan, D. L., Faria, R. T., and Prete, C. E. C.: Evapotranspiration components and dual crop coefficients of coffee trees during crop production, Agr. Water Manage., 98, 791–800, 2011.

Gash, J. H. C., Lloyd, C. R., and Lachaud, G.: Estimating sparse forest rainfall interception with an analytical model, J. Hydrol., 170, 79–86, 1995.

Gelman, A. and Rubin, D. B.: Inference from iterative simulation using multiple sequences, Statistical Sciences, 7, 457–511, 1992.

Hanan, N. P. and Prince, S. D.: Stomatal conductance of west-central supersite vegetation in HAPEX-Sahel: measurements and empirical model, J. Hydrol., 188–189, 536–562, 1997.

Harris, P. P., Huntingford, C., Cox, P. M., Gash, J. H. C., and Malhi, Y.: Effect of soil moisture on canopy conductance of Amazonian rainforest, Agr. Forest Meteorol., 122, 215–227, 2004.

Hastings, W. K.: Monte Carlo sampling methods using Markov chains and their applications, Biometrika, 57, 97–109, 1970.

Hu, Z. M., Yu, G. R., Zhou, Y. L., Sun, X. M., Li, Y. N., Shi, P. L., Wang, Y. F., Song, X., Zheng, Z. M., Zhang, L., and Li, S. G.: Partitioning of evapotranspiration and its controls in four grassland ecosystems: application of a two-source model, Agr. Forest Meteorol., 149, 1410–1420, 2009.

Jarvis, P. G.: The interpretation of the variations in leaf water potential and stomatal conductance found in canopies in the field, Philos. T. R. Soc. B, 273, 563–610, 1976.

Kato, T., Kimura, R., and Kamichika, M.: Estimation of evapotranspiration, transpiration ratio and water-use efficiency from a sparse canopy using a compartment model, Agr. Water Manage., 65, 173–191, 2004.

Korner, C., Schecl, J. A., and Bauer, H.: Maximum leaf diffusive conductance in vascular plants, Phorosynrherica, 13, 45–82, 1979.

Legates, D. R. and McCabe, G. J.: Evaluating the use of "goodness-of-fit" measures in hydrologic and hydroclimatic model validation, Water Resour. Res., 35, 233–241, 1999.

Lemon, E. R., Glaser, A. H., and Satterwhite, L. E.: Some aspects of the relationship of soil, plant, and meteorological factors to evapotranspiration, Proc. Soil Sci. Soc. Amer., 21, 464–468, 1957.

GMDD
7, 741–775, 2014

Lhomme, J. P., Montes, C., Jacob, F., and Prévot, L.: Evaporation from heterogeneous and sparse canopies: on the formulations related to multi-source representations, Bound.-Lay. Meteorol., 144, 243–262, 2012.

Li, S. E., Kang, S. Z., Zhang, L., Ortega-Farias, S., Li, F. S., Du, T. S., Tong, L., Wang, S. F., Ingman, M., and Guo, W. H.: Measuring and modeling maize evapotranspiration under plastic film-mulching condition, J. Hydrol., 503, 153–168, 2013a.

Li, X., Cheng, G. D., Liu, S. M., Xiao, Q., Ma, M. G., Jin, R., Che, T., Liu, Q. H., Wang, W. Z., Qi, Y., Wen, J. G., Li, H. Y., Zhu, G. F., Guo, J. W., Ran, Y. H., Wang, S. G., Zhu, Z. L., Zhou, J., Hu, X. L., and Xu, Z. W.: Heihe Watershed Allied Telemetry Experimental Research (HiWATER): scientific objectives and experimental design1, B. Am. Meteorol. Soc., 94, 1145–1160, 2013b.

Liu, C. M., Zhang, X. Y., and Zhang, Y. Q.: Determination of daily evaporation and evapotranspiration of winter wheat and maize by large-scale weighing lysimeter and micro-lysimeter, Agr. Forest Meteorol., 111, 109–120, 2002.

Liu, S. M., et al.: MUlti-Scale Observation EXperiment on Evapotranspiration over heterogeneous land surfaces (MUSOEXE-12): Flux Observation Matrix, J. Geophys. Res., in preparation, 2014.

Lund, M. R. and Soegaard, H.: Modelling of evaporation in a sparse millet crop using a two-source model including sensible heat advection within the canopy, J. Hydrol., 280, 124–144, 2003.

Metropolis, N. R., Rosenbluth, A. W., Rosenbluth, M. N., and Teller, A. H.: Equations of state calculations by fast computing machines, J. Chem. Phys., 21, 1087–1091, 1953.

Mo, X. G., Lin, Z. H., Xiang, Y. Q., and Liu, S. X.: Characteristics of incoming radiation through maize canopy, Eco-agriculture Research, 8, 1–4, 2000.

Moffat, A. M., Papale, D., Reichstein, M., Hollinger, D. Y., Richardson, A. D., Barr, A. G., Beckstein, C., Braswell, B., Churkina, G., Desai, A. R., Falge, E., Gove, J. H., Heimann, M., Hui, D., Jarvis, A. J., Kattge, J., Noormets, A., and Stauch, V. J.: Comprehensive comparison of gap-flling techniques for eddy covariance net carbon fluxes, Agr. Forest Meteorol., 147, 209–232, 2007.

Morison, J. I. L., Baker, N. R., Mullineaux, P. M., and Davies, W. J.: Improving water use in crop production, Philos. T. R. Soc. B, 363, 639–658, 2008.

Mulder, J. P. M.: Simulating interception loss using standard meteorological data, in: The Forest-Atmosphere Interaction, edited by: Hutchison, B., Hicks, B., and Reidel, D., 177–196, 1985.

GMDD
7, 741–775, 2014

Noilhan, J. and Planton, S.: A simple parameterization of land surface processes for meteorological Models, Mon. Weather Rev., 117, 536–549, 1989.
Ogink-Hendriks, M. J.: Modelling surface conductance and transpiration of an oak forest in the Netherlands, Agr. Forest Meteorol., 74, 99–118, 1995.
Ortega-Farias, S., Carrasco, M., Olioso, A., Acevedo, C., and Poblete, C.: Latent heat flux over a Cabernet Sauvignon vineyard using the Shuttleworth and Wallace model, Irrigation Sci., 25, 161–170, 2007.
Ortega-Farias, S., Poblete-Echeverria, C., and Brisson, N.: Parameterization of a two-layer model for estimating vineyard evapotranspiration using meteorological measurements, Agr. Forest Meteorol., 150, 276–286, 2010.
Poblete-Echeverria, C. and Ortega-Farias, S.: Estimation of actual evapotranspiration for a drip-irrigated Merlot vineyard using a three-source model, Irrigation Sci., 28, 65–78, 2009.
Pospisilova, J. and Solarova, J.: Environmental and biological control of diffusive conductance of adaxial and abaxial leaf epidermis, Photosyntherica, 14, 90–127, 1980.
Rana, G. and Katerji, N.: Measurement and estimation of actual evapotranspiration in the field under Mediterranean climate: a review, Eur. J. Agron., 13, 125–153, 2000.
Rao, K., Wyngaard, J., and Cote, O.: Local advection of momentum, heat, and moisture in micrometeorology, Bound.-Lay. Meteorol., 7, 331–348, 1974.
Rutter, A. J., Kershaw, K. A., Robbins, P. C., and Morton, A. J.: A predictive model of rainfall interception in forests, I. Derivation of the model from observations in a plantation of Corsican pine, Agr. Forest Meteorol., 9, 367–384, 1971.
Samanta, S., Mackay, D. S., Clayton, M. K., Kruger, E. L., and Ewers, B. E.: Bayesian analysis for uncertainty estimation of a canopy transpiration model, Water Resour. Res., 43, W04424, doi:10.1029/2006WR005028, 2007.
Scott, R. L., Huxman, T. E., Cable, W. L., and Emmerich, W. E.: Partitioning of evapotranspiration and its relation to carbon dioxide exchange in a Chihuahuan desert shrubland, Hydrol. Process., 20, 3227–3243, 2006.
Sellers, P. J., Heiser, M. D., and Hall, F. G.: Relations between surface conductance and spectral vegetation indices at intermediate (100 m^2 to 15 km^2) length scales, J. Geophys. Res., 97, 19033–19059, 1992.
Shuttleworth, W. J. and Gurney, R. J.: The theoretical relationship between foliage temperature and canopy resistance in sparse crops, Q. J. Roy. Meteor. Soc., 116, 497–519, 1990.

GMDD
7, 741–775, 2014

Shuttleworth, W. J. and Wallace, J. S.: Evaporation from sparse crops- an energy combination theory, Q. J. Roy. Meteor. Soc., 111, 839–855, 1985.
Stannard, D. I.: Comparison of Penman–Monteith, Shuttleworth–Wallace and modified Priestley–Taylor evapotranspiration models for wildland vegetation in semiarid rangeland, Water Resour. Res., 29, 1379–1392, 1993.
Stewart, J. B.: Modelling surface conductance of pine forest, Agr. Forest Meteorol., 43, 19–35, 1988.
Sun, H. Y., Shao, L. W., Liu, X. W., Miao, W. F., Chen, S. Y., and Zhang, X. Y.: Determination of water consumption and the water-saving potential of three mulching methods in a jujube orchard, Eur. J. Agron., 43, 87–95, 2012.
Sun, S. F.: Moisture and heat transport in a soil layer forced by atmospheric conditions, MS thesis, University of Connecticut, 1982.
Svensson, M., Jansson, P. E., Gustafson, D., Kleja, D. B., Langvall, O., and Lindroth, A.: Bayesian calibration of a model describing carbon, water and heat fluxes for a Swedish boreal forest stand, Ecol. Model., 213, 331–344, 2008.
Teh, C. B. S., Simmonds, L. P., and Wheeler, T. R.: Modelling the partitioning of solar radiation capture and evapotranspiration intercropping systems, in: Proceedings of the 2nd International Conference on Tropical Climatology, Meteorology and Hydrology TCMH-2001, Brussels, Belgium, 2001.
Tourula, T. and Heikinheimo, M.: Modelling evapotranspiration from a barley field over the growing season, Agr. Forest Meteorol., 91, 237–250, 1998.
van de Griend, A. A. and Owe, M.: Bare soil surface resistance to evaporation by vapor diffusion under semiarid conditions, Water Resour. Res., 30, 181–188, 1994.
van Oijen, M., Rougier, J., and Smith, R.: Bayesian calibration of process-based forest models: bridging the gap between models and data, Tree Physiol., 25, 915–927, 2005.
Verhoef, A. and Allen, S. J.: A SVAT scheme describing energy and CO_2 fluxes for multi-component vegetation: calibration and test for a Sahelian savannah, Ecol. Model., 127, 245–267, 2000.
Verhoef, A., Fernández-Gálvez, J., Diaz-Espejo, A., Main, B. E., El-Bishti, M. The diurnal course of soil moisture as measured by various dielectric sensors: effects of soil temperature and the implications for evaporation estimates, J. Hydrol., 321, 147–162, 2006.
Verhoef, A., Ottle, C., Cappelaere, B., Murray, T., Saux-Picart, S., Zribi, M., Maignan, F., Boulain, N., Demarty, J., and Ramier, D.: Spatio-temporal surface soil heat flux estimates

GMDD
7, 741–775, 2014

from satellite data: results for the AMMA experiment at the Fakara (Niger) supersite, Agr. Forest Meteorol., 154–155, 55–66, 2012.
Villagarcía, L., Were, A., García, M., and Domingo, F.: Sensitivity of a clumped model of evapotranspiration to surface resistance parameterisations: application in a semi-arid environment, Agr. Forest Meteorol., 150, 1065–1078, 2010.
Wallace, J. S. and Verhoef, A.: Interactions in mixed-plant communities: light, water and carbon dioxide, in: Leaf Development and Canopy Growth, edited by: Marshall, B. and Roberts, J. A., Sheffield Biological Science Series, Sheffield Academic Press, Sheffield, 204–250, 2000.
Wang, J. M. and Mitsuta, Y.: Evaporation from the desert: some preliminary results of HEIFI, Bound.-Lay. Meteorol., 59, 413–418, 1992.
Wang, X. F. and Yakir, D.: Using stable isotopes of water in evapotranspiration studies, Hydrol. Process., 14, 1407–1421, 2000.
Williams, D. G., Cable, W., Hultine, K., Hoedjes, J. C. B., Yepez, E. A., Simonneaux, V., Er-Raki, S., Boulet, G., de Bruin, H. A. R., Chehbouni, A., Hartogensis, O. K., and Timouk, F.: Evapotranspiration components determined by stable isotope, sap flow and eddy covariance techniques, Agr. Forest Meteorol., 125, 241–258, 2004.
Xu, Z. W., Liu, S. M., Li, X., Shi, S. J., Wang, J. M., Zhu, Z. L., Xu, T. R., Wang, W. Z., and Ma, M. G.: Intercomparison of surface energy flux measurement systems used during the HiWATER-USOEXE, J. Geophys. Res., 118, 13140–13157, doi:10.1002/2013JD020260, 2014.
Zhang, B. Z., Kang, S. Z., Li, F. S., and Zhang, L.: Comparison of three evapotranspiration models to Bowen ratio-energy balance method for a vineyard in an arid desert region of northwest China, Agr. Forest Meteorol., 148, 1629–1640, 2008.
Zhang, Q. and Huang, R. H.: Water vapor exchange between soil and atmosphere over a Gobi surface near an oasis in Summer, J. Appl. Meteorol., 43, 1917–1928, 2004.
Zhang, X.: Improvement of a soil-atmosphere-transfer model for the simulation of bare soil surface energy balances in semiarid areas, Asia-Pac. J. Atmos. Sci., 48, 97–105, 2012.
Zhu, G. F., Li, Z. Z., Su, Y. H., Ma, J. Z., and Zhang, Y. Y.: Hydrogeochemical and isotope evidence of groundwater evolution and recharge in Minqin Basin, northwest China, J. Hydrol., 333, 239–251, 2007.
Zhu, G. F., Su, Y. H., and Feng, Q.: The hydrochemical characteristics and evolution of groundwater and surface water in the Heihe River Basin, northwest China, Hydrogeol. J., 16, 167–182, 2008.

GMDD
7, 741–775, 2014

Zhu, G. F., Li, X., Su, Y. H., Lu, L., and Huang, C. L.: Seasonal fluctuations and temperature dependence in photosynthetic parameters and stomatal conductance at the leaf scale of *Populus euphratica Oliv.*, Tree Physiol., 31, 178–195, 2011.

Zhu, G. F., Su, Y. H., Li, X., Zhang, K., and Li, C. B.: Estimating actual evapotranspiration from an alpine grassland on Qinghai-Tibetan plateau using a two-source model and parameter uncertainty analysis by Bayesian approach, J. Hydrol., 476, 42–51, 2013.

GMDD

7, 741–775, 2014

Table 1. Prior distributions and the parameter bounds for the S–W model. These values are derived from the literature; the posterior parameter distribution estimated by MCMC are based on observed data in our site, and are characterized by the mean and 95 % high-probability intervals (Lower limit, Upper limit).

Parameter	Prior Distribution			Posterior Distribution	
	Lower Bound	Upper Bound	References	Mean	95 % High-Probability Interval
r_{STmin} (sm^{-1})	0	80	Noilhan and Planton (1989); Li et al. (2013a)	**21.8**	(20.2, 24.6)
k_1 (Wm^{-2})	0	500	Stewart (1998)	294.6	(42.5, 487.7)
k_2 (°C)	5	40	Ogink-Hendriks (1995)	**25.6**	(12.9,34.4)
k_3 (kPa^{-1})	0	0.1	Stewart (1998)	0.02	(0, 0.07)
b_1 (sm^{-1})	4	15	Sellers et al. (1992); Zhang (2012); Zhu et al. (2013)	**9.3**	(8.4, 10.0)
b_2 (sm^{-1})	0	8	Sellers et al. (1992); Zhang (2012) ; Zhu et al. (2013)	**6.2**	(3.8, 7.4)

The bold number means that this parameter was well constrained by the data.

GMDD
7, 741–775, 2014

Table 2. Statistical analysis of measured and estimated values of half-hourly evapotranspiration (λET; $W m^{-2}$), daily soil evaporation (E; $mm d^{-1}$), and daily evapotranspiration (ET; $mm d^{-1}$) for the spring maize in arid desert oasis during the study period.

	n	Regressive equation	R^2	Mean measured values	Mean simulated values	RMSE	MBE	IA	EF
λET ($W m^{-2}$)	3578	$\lambda ET_{modeled} = 0.84 \lambda ET_{measured} + 0.18$	0.83	161.4	137.2	80.7	24.2	0.93	0.74
E ($mm d^{-1}$)	56	$E_{modeled} = 1.01 E_{measured} + 0.01$	0.82	0.26	0.28	0.05	−0.01	0.94	0.76
ET ($mm d^{-1}$)	95	$ET_{modeled} = 0.83 ET_{measured} + 0.19$	0.83	2.02	1.88	0.32	0.14	0.94	0.79

n = the sample number; R^2 = the determination coefficient; RMSE = root mean square error; MBE = mean bias error between measured and modeled values; IA = index of agreement; ET = model efficiency. These statistical parameters are calculated using formulas given by Legates and McCabe (1999) and Poblete-Echeverria and Ortega-Farias (2009).

GMDD
7, 741–775, 2014

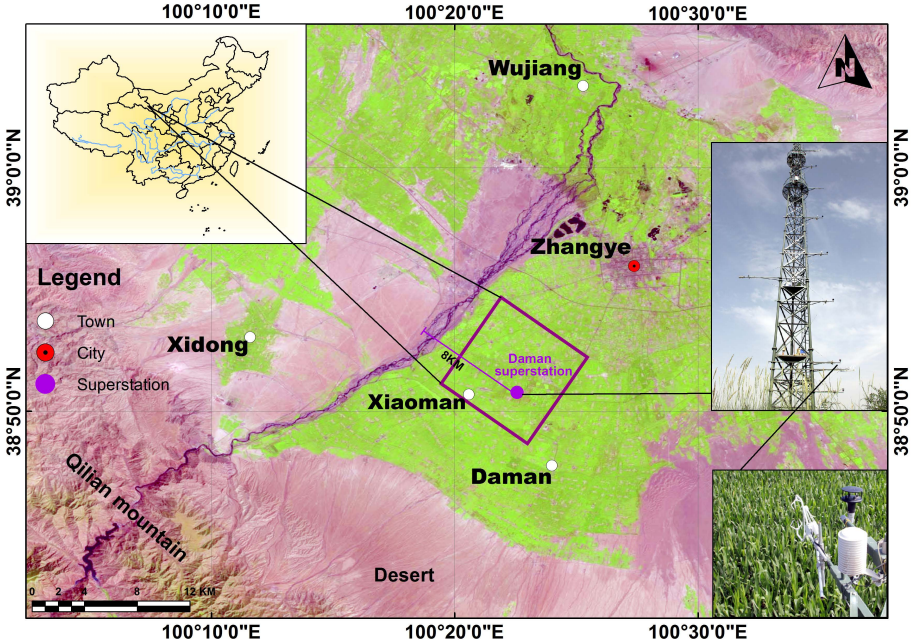

Fig. 1. Experimental location and instrumentation setting at Daman (DM) superstation.

GMDD
7, 741–775, 2014

Simultaneously parameterize the ET model by Bayesian approach

G. F. Zhu et al.

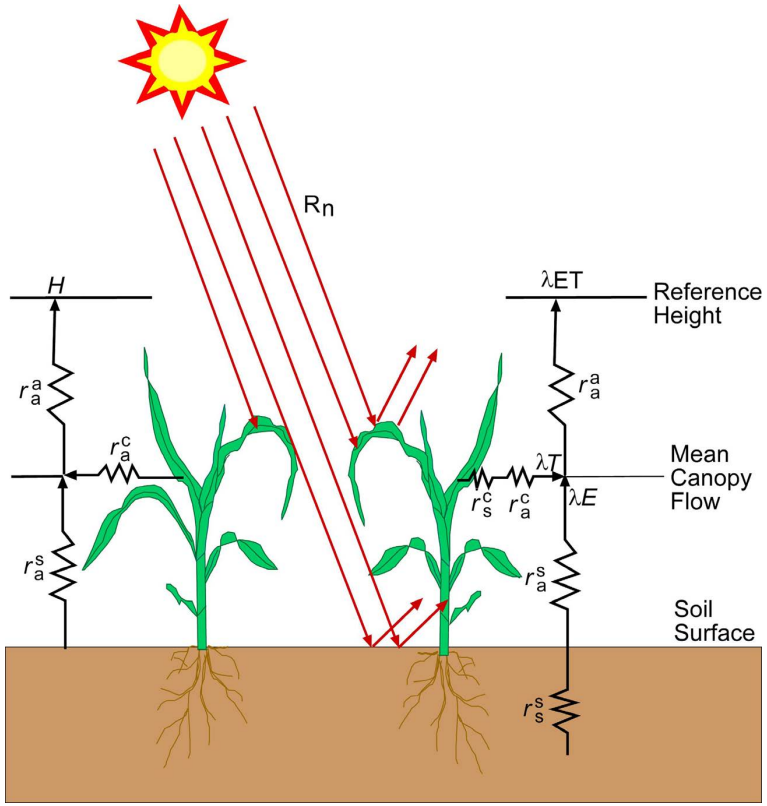

Fig. 2. Schematic diagram of the S–W model. From right to left, r_s^c and r_a^c are bulk resistances of canopy stomatal and boundary layer ($s\,m^{-1}$), respectively; r_a^s and r_a^a aerodynamic resistances from soil to canopy and from canopy to reference height ($s\,m^{-1}$), respectively; r_s^s soil surface resistance ($s\,m^{-1}$). λT transpiration from canopy ($W\,m^{-2}$), λE evaporation from soil under plant ($W\,m^{-2}$), and λET total evapotranspiration ($W\,m^{-2}$).

GMDD
7, 741–775, 2014

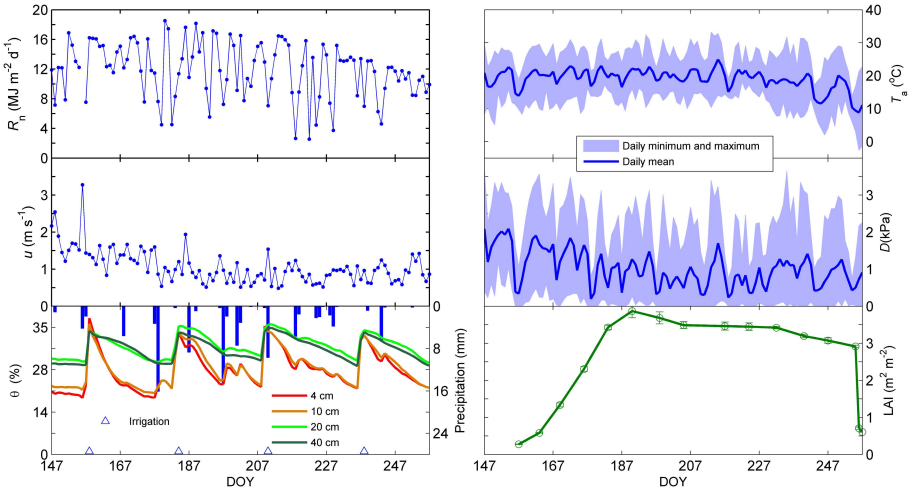

Fig. 3. Seasonal variation in net solar radiation (R_n; MJ m^{-2} d^{-1}), air temperature (T_a; °C), vapor pressure deficit (D; kPa), wind speed (u; m s^{-1}) at the height of 3 m, precipitation and irrigation (mm), soil water content (θ; m^3 m^{-3}) and leaf are index (LAI; m^2 m^{-2}) during the study period in the Daman Oasis.

GMDD
7, 741–775, 2014

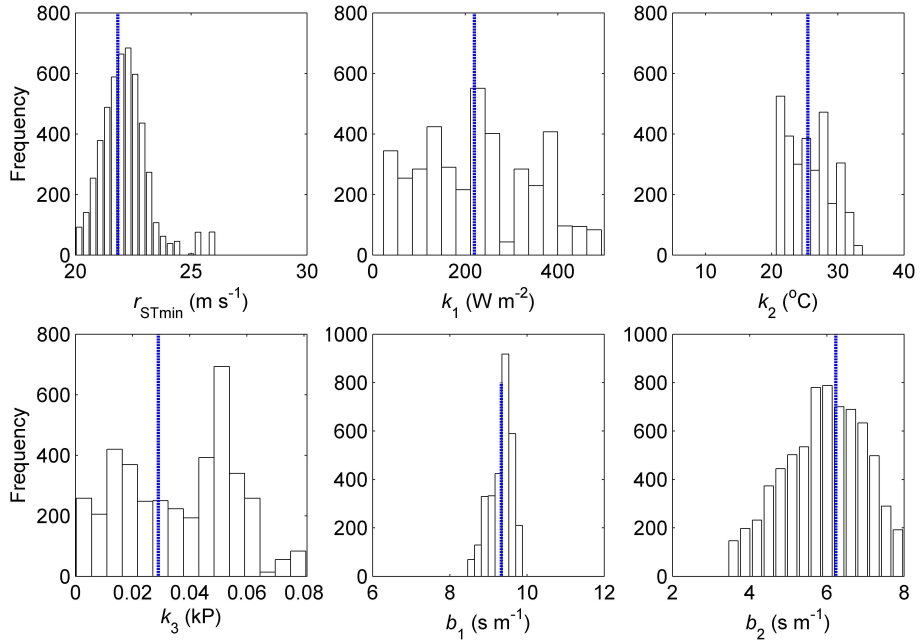

Fig. 4. Histograms of samples from the posterior distributions of the parameters. The dashed vertical lines indicate mean parameter values.

GMDD
7, 741–775, 2014

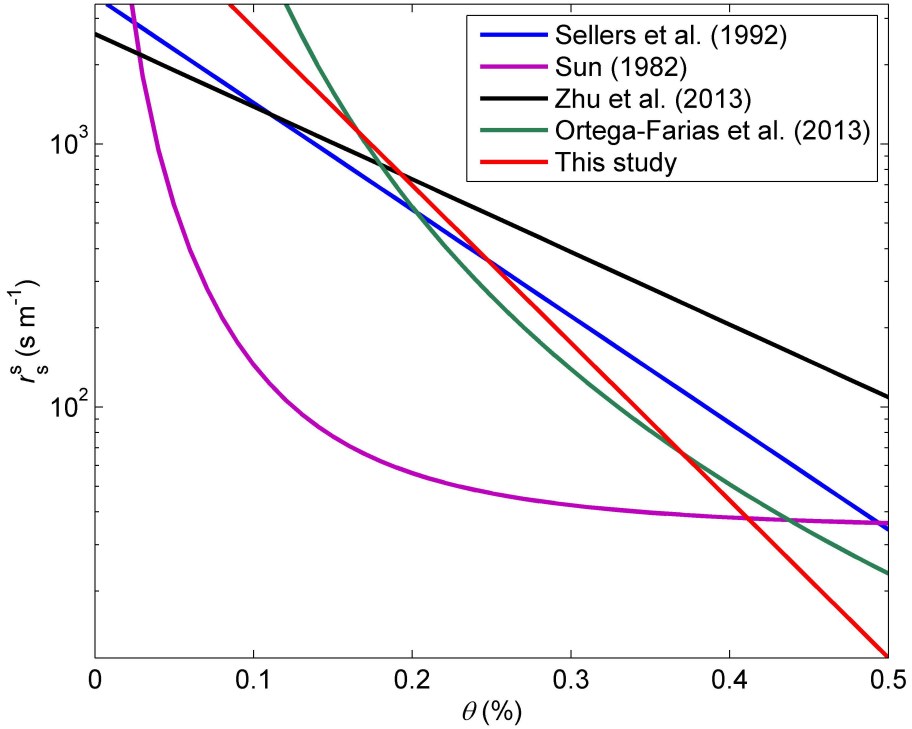

Fig. 5. Comparisons of responses of soil surface resistance (r_s^s s m^{-1}) to soil surface water contents (θ; m^3 m^{-3}).

GMDD
7, 741–775, 2014

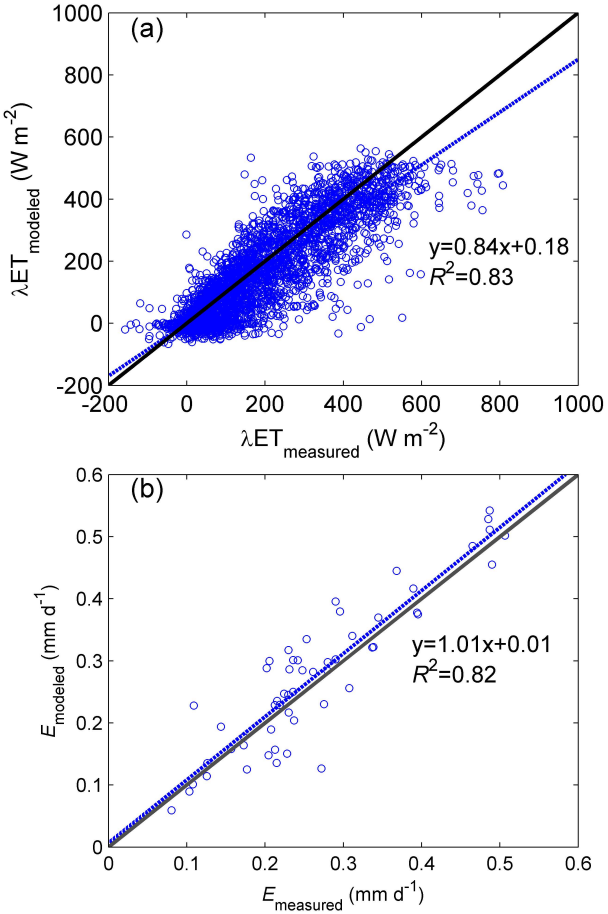

Fig. 6. (a) Plot of estimated evapotranspiration (λET; W m^{-2}) against observed values. The regressions is: $y = 0.84x + 0.18$ ($R^2 = 0.83$); **(b)** plot of estimated daily soil evaporation (E; mm d^{-1}) against measured data. The regressions is: $y = 1.01x + 0.01$ ($R^2 = 0.82$).

GMDD
7, 741–775, 2014

Simultaneously parameterize the ET model by Bayesian approach

G. F. Zhu et al.

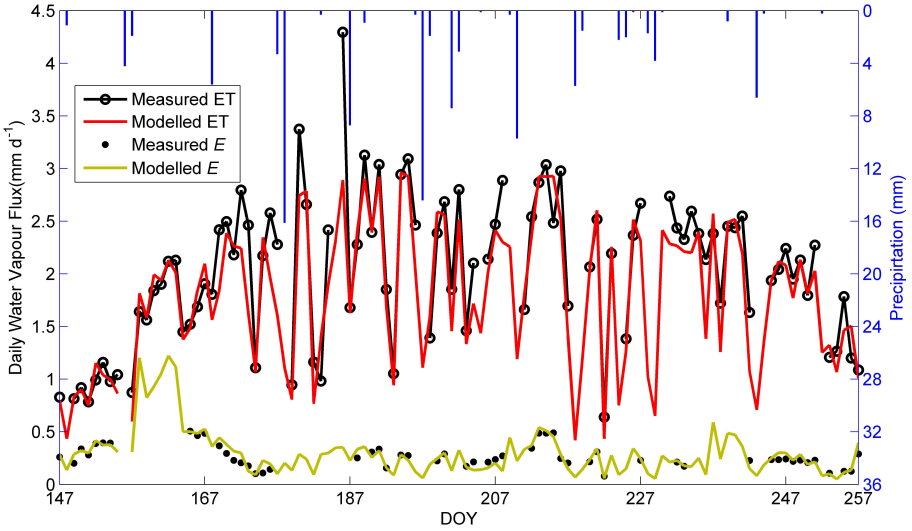

Fig. 7. Seasonal variation in daily evapotranspiration (ET; mm d^{-1}) and soil evaporation (E; mm day^{-1}) measured by the EC system and microlysimeters and modeled by the S–W model during the study period in Daman Oasis. Gap in the time series is caused either by the absence of flux measurements or missing ancillary data.

GMDD
7, 741–775, 2014

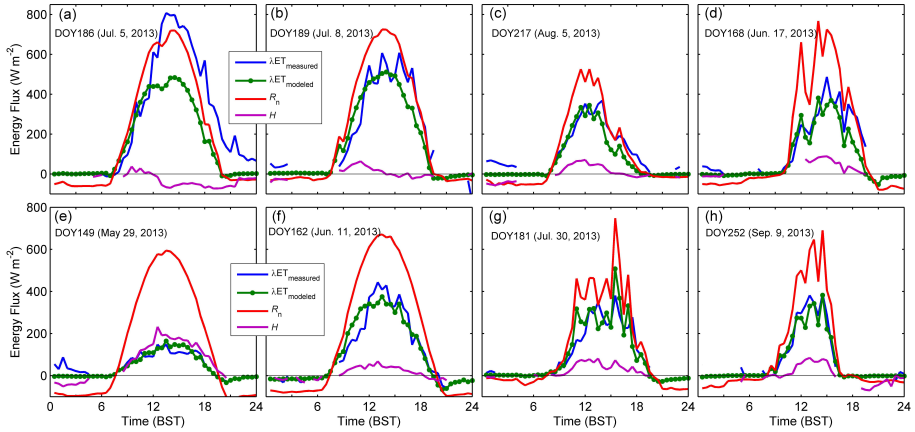

Fig. 8. Diurnal variations in net radiation flux (R_n; $W m^{-2}$), sensible heat flux (H; $W m^{-2}$), and modeled and measured evapotranspiration flux (λET; $W m^{-2}$). **(a)–(c)** Represented conditions at which micro-scale advection occurred at 12:00, 15:00 and 17:00 Beijing Standard Time (BST), respectively, **(d)** represented a rainy day, and **(e)–(h)** represented clear and advection-absent days during the study period. Gap is caused either by the absence of flux measurements or missing ancillary data.

GMDD
7, 741–775, 2014

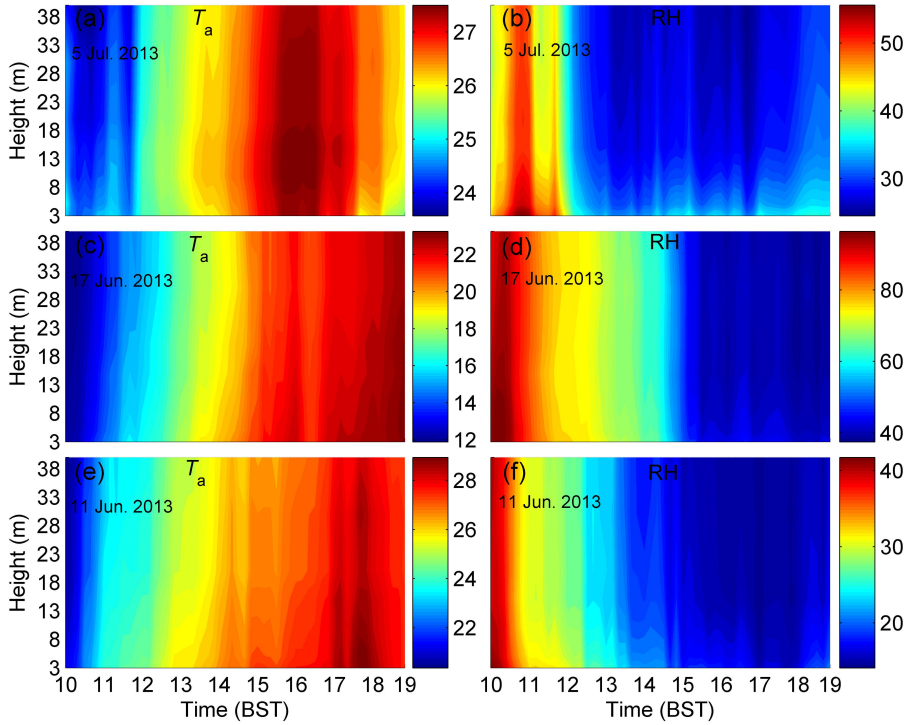

Fig. 9. The diurnal evolutions of temperature (T_a; ˚C) and relative humidity (RH; %) profiles from 3 m to 40 m above the ground. Profiles of **(a)** T_a and **(b)** RH on 5 July, 2013. An obvious advection process can be detected from 13:00 to 17:00 BST with high T_a and low RH layer at the height of 8–18 m; profiles of **(c)** T_a and **(d)** RH on 17 June, 2013. A precipitation event occurred at 13:00 and resulted in uniform vertical distributions of Ta and RH, but no temperature inversion were observed; profiles of **(e)** T_a and **(f)** RH on 11 June, 2013. It represented a typical clear and advection-absent day.

GMDD
7, 741–775, 2014